A dopaminergic memory circuit controls acute valence

Farhan Mohammad [1, 5, *], Yishan Mai [1, *], Joses Ho [2], Xianyuan Zhang [3], Stanislav Ott [1], James Charles Stewart [2], & Adam Claridge-Chang [1, 2, 4, 6]

1. Program in Neuroscience and Behavioural Disorders, Duke-NUS Medical School, Singapore.
2. Institute for Molecular and Cell Biology, A*STAR, Singapore.
3. Department of Pharmacology, National University of Singapore, Singapore.
4. Department of Physiology, National University of Singapore, Singapore.
5. Division of Biological and Biomedical Sciences, College of Health & Life Sciences, Hamad Bin Khalifa University, Qatar.
6. Correspondence: claridge-chang.adam@duke-nus.edu.sg
* Equal contribution

Abstract

The brain must guide immediate responses to beneficial and harmful stimuli while simultaneously writing memories for future reference. Both immediate actions and reinforcement learning are instructed by dopamine. However, it is unknown how dopaminergic systems maintain coherence between these two reward functions. Optogenetic activation experiments showed that the dopamine neurons that inform olfactory memory in *Drosophila* have a distinct, parallel function driving attraction and aversion (valence). Olfactory-memory neurons were dispensable for valence. A broadly projecting set of dopaminergic cells had valence that was dependent on dopamine, glutamate, and octopamine. Similarly, a more restricted dopaminergic cluster with attractive valence was reliant on dopamine and glutamate. Opto-inhibition of this narrow subset revealed that behavior was influenced by pre-existing dopaminergic activity. Dopamine's acute effect on valence provides a mechanism by which a dopaminergic circuit can coherently write memories to influence future responses while guiding immediate actions.

Keywords

Motivation, Reward, Valence, Reinforcement, Locomotion, Synapse, Dopamine

Table of Contents

Introduction

For an animal to survive and thrive, its brain must integrate sensory stimuli and internal signals to guide it toward benefits and away from harm. Some neural information has evolved to be innately instructive to behavior—for example, a sensory response to painful heat. Other information has no inherent evolutionary imperative *a priori*, but can acquire behavioral meaning through learning. A fundamental aspect of all brain states is their propensity to make an animal approach or avoid a stimulus, a property termed 'emotional valence' [1]. In humans, an emotional behavior like a facial expression of disgust is characterized as having negative valence, while a happy smile can be said to have positive valence. It has long been appreciated that such emotional behaviors have counterparts in all animals, including insects [1–3]. In the brain, emotional valence is partly governed by neuromodulators, soluble factors that modify neuronal excitability and synaptic dynamics through their action on metabotropic receptors [4]. Through these cellular effects, neuromodulators transform circuit dynamics, eliciting various motor outputs from a single network [5].

One particularly important neuromodulator is dopamine. In mammals, dopamine-releasing cells have been implicated in diverse processes that include motor function, motivation, associative learning and acute valence [6–8]. Many of these functions are conserved across animal species, including the experimentally-tractable vinegar fly, *Drosophila melanogaster.* Studies in flies have verified dopamine's importance in sleep [9–11], reward conditioning [12–14], courtship [15], aversive learning [16,17], and olfactory memories formed within the mushroom body (MB) [12,13,17–21].

The synaptic fields of the MB are formed from the confluence of ~2000 odor-responsive sensory Kenyon cells (KCs), 34 mushroom-body output neurons (MBONs), and ~120 dopaminergic cells (DANs) [22]. Dopamine release modulates the weights of synapses between the KCs and the MBONs [23,24], assigning negative or positive valence to an odor response when coincident events activate aversive or appetitive DANs, respectively [25]. In addition to this associative role, certain MB DANs are required for innate preference behavior [14], can acutely drive valent behavior, and form direct contacts with the MBONs [26], activity wherein is sufficient to drive avoidance and attraction [27].

Both DANs and KCs synapse with MBONs [28], which affect behavioral valence by influencing locomotion [27]. Changes in olfactory valence arise when DANs modulate KC→MBON synaptic strength [23–25]. DAN activity itself is also reported

to drive valence [26,28], but, relative to dopamine's diverse roles in olfactory conditioning [12,14,16,18,29–39], this behavior has been less explored.

In the present study, we used optogenetic activation experiments, in which freely-moving flies bearing optogenetic constructs were allowed to approach or avoid artificial activation of genetically defined dopaminergic cells. We found that flies are attracted to or avoid select dopaminergic activities, but are largely indifferent to others. Genetic lesions indicate that dopaminergic acute valence is independent of MB sensory and associative functions, suggesting that this behavior is distinct from learning. In a broad driver, valence depends on dopamine, glutamate and octopamine; in the β-lobe DANs, valence depends on both dopamine and glutamate, establishing roles for co-transmitters. An optogenetic inhibition experiment of the β-lobe DANs revealed that, even in a low-stimulus environment, pre-existing neural activity contributes to ongoing locomotor behavior.

Results

Mushroom-body dopamine neurons drive approach and avoidance

To investigate the role of dopamine on acute approach/avoidance behaviors, we generated transgenic flies expressing an optogenetic activator (Chrimson, henceforth 'Chr') [40] in the paired-anterior-medial dopaminergic neurons (PAM DANs) that project to the MB [12,13,41]. The flies were then analyzed in a light-dark choice assay (**Figure 1A**). The *R58E02* is a fusion of a flanking region of the *Dopamine transporter* (*DAT*) gene fused with *Gal4* [42,43]. This driver expresses in a large subset of the PAM DANs, and has fibers in a broad set of MB neuropil zones [12,13,35,36,44,45] (**Figure 1B, S1A**). Valence was calculated as an effect size calculated as the mean difference between optogenetic test flies and the corresponding controls, and displayed as effect-size curves [46]. Flies expressing the Chr opto-activator with the *R58E02* transgene were strongly attracted to light (**Figure 1E, Movie S1**). By contrast, another driver, *R15A04*, expressed in PAM DANs that send fibers to a more restricted set of MB zones [36,43,45] (**Figure 1C, S1B**). These *R15A04>Chr* flies tended to avoid the light at the highest illumination intensity (70 μM/mm^2, **Figure 1F**). Thus, while activation of the *R58E02* DANs drives strong positive valence, flies will avoid activation in the subset defined by *R15A04*.

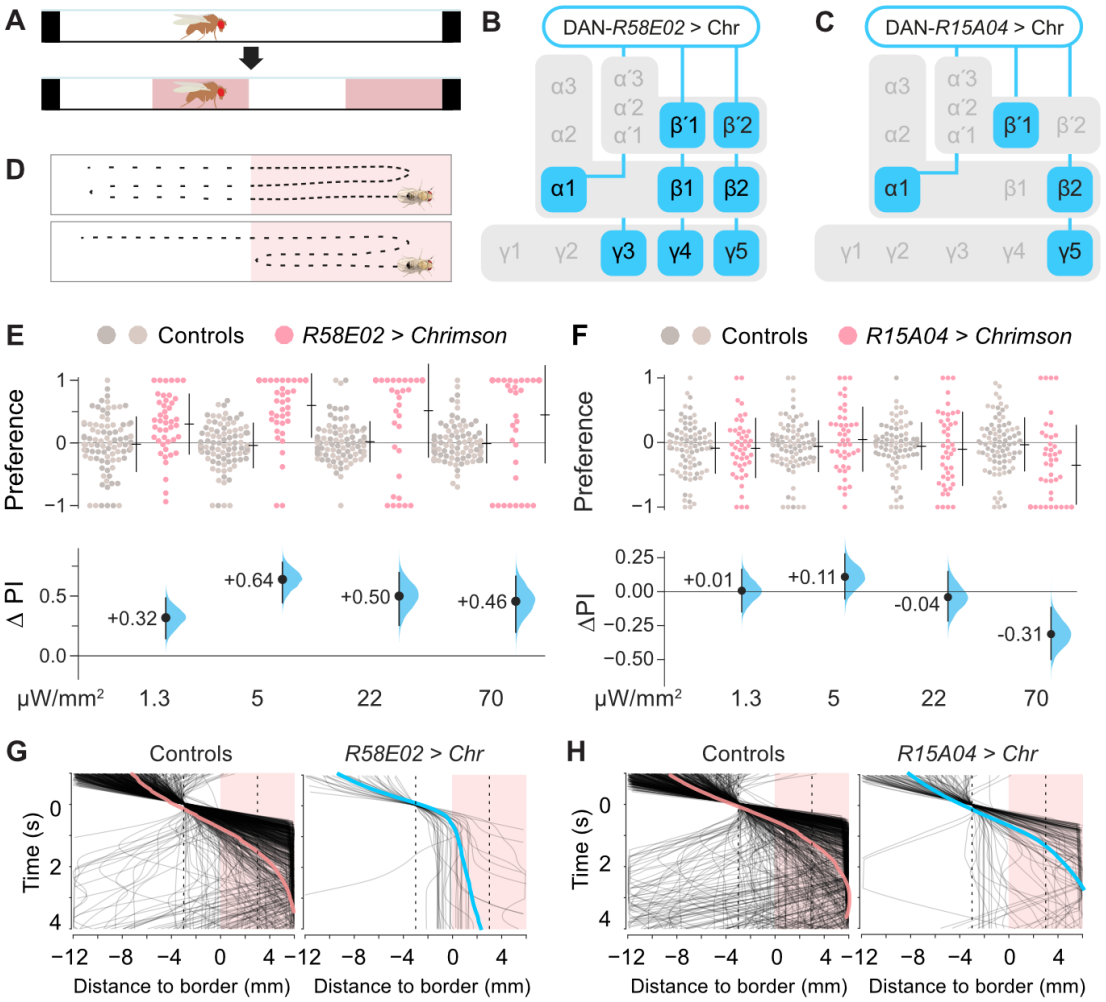

Figure 1. Activities in different dopaminergic cells drive valence

A. Optogenetic assay schematic showing that, after an initial dark phase, half of the chamber is illuminated with two bands of red light. See Methods for further details.

B–C. A schematic summary of two DAN drivers, *R58E02* and *R15A04*, with projections to MB synaptic zones. *R58E02* expresses in nearly all the PAM types, projecting to α1, β1, β2, β'1, β'2, γ4, and γ5, with weaker expression in γ1, γ2, and the peduncle. *R15A04* expresses in PAMs that project to the α1, β2, β'1, and γ5 zones.

D. Schematic of hypothetical locomotor modes for valence. **Top** Flies move slowly in the favored area. **Bottom** Flies maneuver to remain in the favored area. Either mode increases the time spent in the preferred area.

E. *R58E02>Chr* flies spent more time in the light zones. The **upper panel** shows the preference indices (PIs) for test flies (red dots) and driver and responder controls (*R58E02*/+ and *Chr*/+, gray dots). The **lower panel** shows the valence effect sizes (mean differences, ΔPI) between control and test flies, with confidence intervals

(black line) and the distribution of ΔPI error (blue curve). The positive ΔPI values indicate a positive valence. See **Table S1** for detailed genotypes and statistics.

F. *R15A04>Chr* flies avoided opto-activation. The negative ΔPI values indicate avoidance.

G. Walking behavior of the subset of flies that entered the choice zonet from the dark side, as they approach the dark–light interface. Traces of *R58E02>Chr* paths (black) are aligned to choice-zone entry, i.e. locked to the time of entering the boundary area. The colored lines show the overall mean trajectory. The horizontal axis is aligned to the middle of the choice zone. Test flies slowed or stopped at the boundary, with their heads on either side of the middle of the light interface.

H. Traces of *R15A04>Chr* flies as they enter the choice zone from the dark side. Trajectory data were taken from epochs with 70 µW/mm illumination.

DAN activation influences locomotion

When traversing a boundary between two stimulus areas, walking flies encountering aversive stimuli or an aversive odor use reversals or turns to maneuver away [18,27]. However, a fly displaying a spatial preference for one of two areas could hypothetically employ another locomotor mode: slowing down in the favored area (**Figure 1D**). We explored how valence, choice, and speed were associated in *R58E02* and *R15A04* flies. Regressions between preference, speed ratio, and a choice index showed that, in these lines preference was more strongly determined by differential speed (**Figure S1C-F**). We also inspected locomotion at the boundary by aligning the dark-to-light trajectories in a single experiment. In the subset of flies that entered the boundary choice-zone, trajectory lines drawn over time indicated that, as the optogenetic DAN lines traverse into the choice zone from the dark side, the *R58E02>Chr* flies tend to walk slower and frequently stop in the boundary area (**Figure 1G-H**). These observations suggest that these groups of DANs affect valence via walking-speed changes.

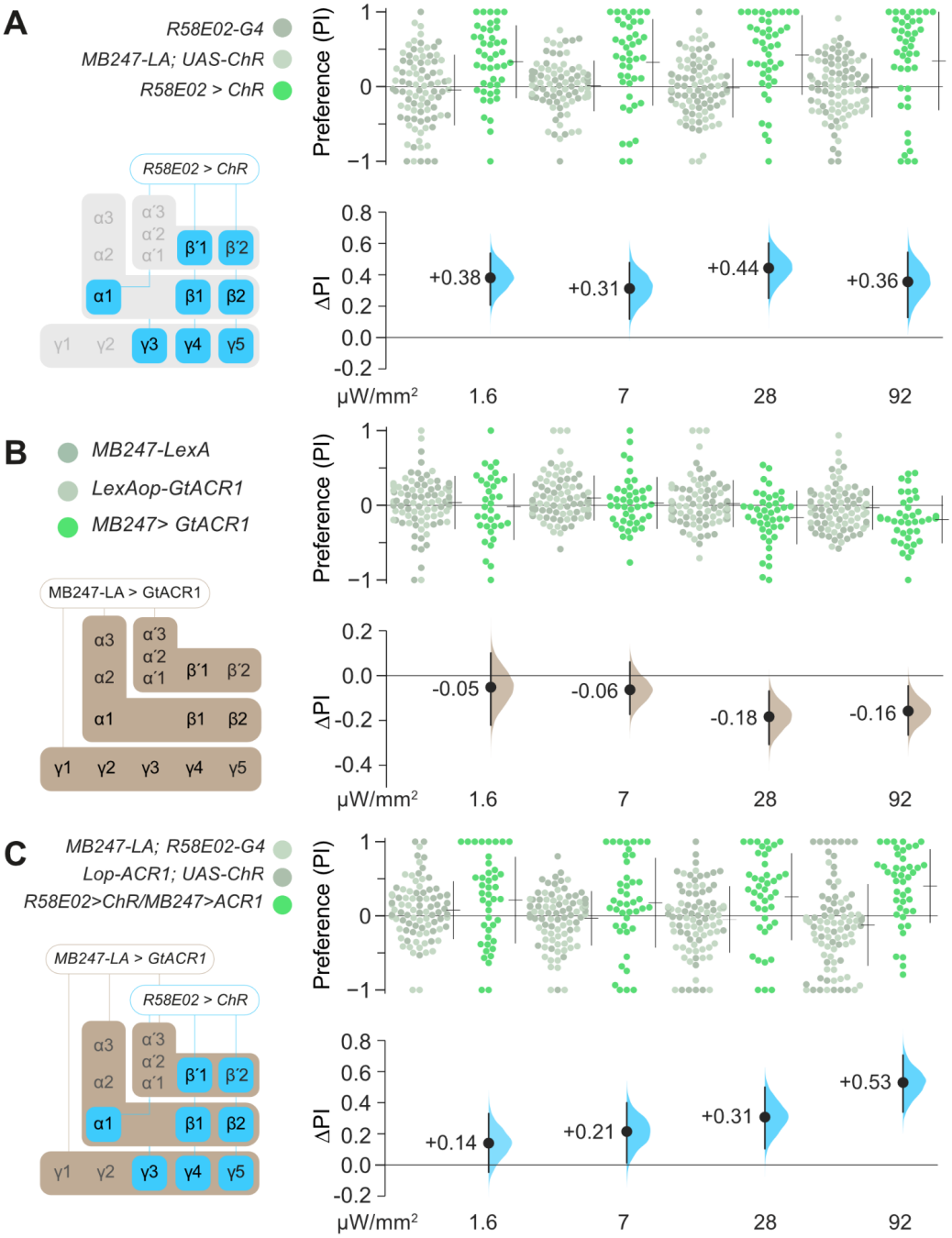

Figure 2. Kenyon cells are dispensable for *R58E02* DAN valence.

A. *R58E02>Chr* flies are attracted to green light. Left schematic illustrates the expression pattern of *R58E02*. Flies carrying all three transgenes displayed attraction to green light (green dots), resulting in positive valence (black dots and blue curves in the lower panel). Parental-type control flies (*R58E02-Gal4/+* or *MB247-LexA/+; UAS-Chr/+*, gray dots) showed a neutral preference for green light.

B. Relative to genetic controls, *MB247-LexA>lexAop-ACR1* flies display a modest avoidance of green light at high intensities (22 and 72 μW/mm²). Schematic

indicates that *MB247-LexA* drives expression of ACR in a majority of MB intrinsic Kenyon cells.

C. In *R58E02>Chr/MB247>ACR1* flies, preference for DAN activation mediated by *R58E02-Gal4>UAS-Chr* is unaffected by simultaneous opto-inhibition of the MB intrinsic cells with *MB247-LexA>lexAop-ACR1*. Effect sizes (blue curves) show the net effect of comparing test flies carrying all four transgenes (green dots) with controls (gray dots).

The Kenyon cells are dispensable for broad DAN attraction

DANs instruct odor memory by modulating KC function [23,25]. We thus asked whether, like memory, DAN optogenetic valence relies on KC activity [47,48]. We implemented a strategy to allow flies to simultaneously activate DANs with Chr and inhibit KCs using the light-actuated anion channelrhodopsin, GtACR1 (hereon 'ACR1') [49,50]. As both channelrhodopsins are responsive to green light, we tested the ability of green light to both activate DANs and silence KCs. *R58E02>Chr* flies were attracted to green light (**Figure 2A, S2A**), confirming effective Chr actuation. One possible confound would be if flies responded to KC inhibition with a strong attraction that masked DAN attraction; however, in a valence test, *MB247>ACR1* flies exhibited only mild aversion (**Figure 2B**). With aversive shock–odor conditioning under green light (**Figure S2E**), flies expressing the opto-inhibitor in the KCs (*MB247>ACR1*) failed to learn (**Figure S2F**), demonstrating that ACR1 sufficiently inhibits KCs to abolish memory formation. In *R58E02>Chr* flies, green light successfully induced optogenetic appetitive memories; however, in *R58E02>Chr, MB247>ACR1* flies, green light did not induce synthetic memory (**Figure S2G**), further verifying that ACR1 elicits KC inhibition. Flies carrying the *R58E02>Chr, MB247>ACR1* genotype were then tested for their optogenetic preference; even with inhibited KCs, valence remained intact (**Figure 2C, S2B**). Additional control experiments also showed that the olfactory receptor neurons are not required for PAM valence (**Figure S2CD**). These results indicate that, for PAM-mediated attraction, olfactory input and KC activity are dispensable.

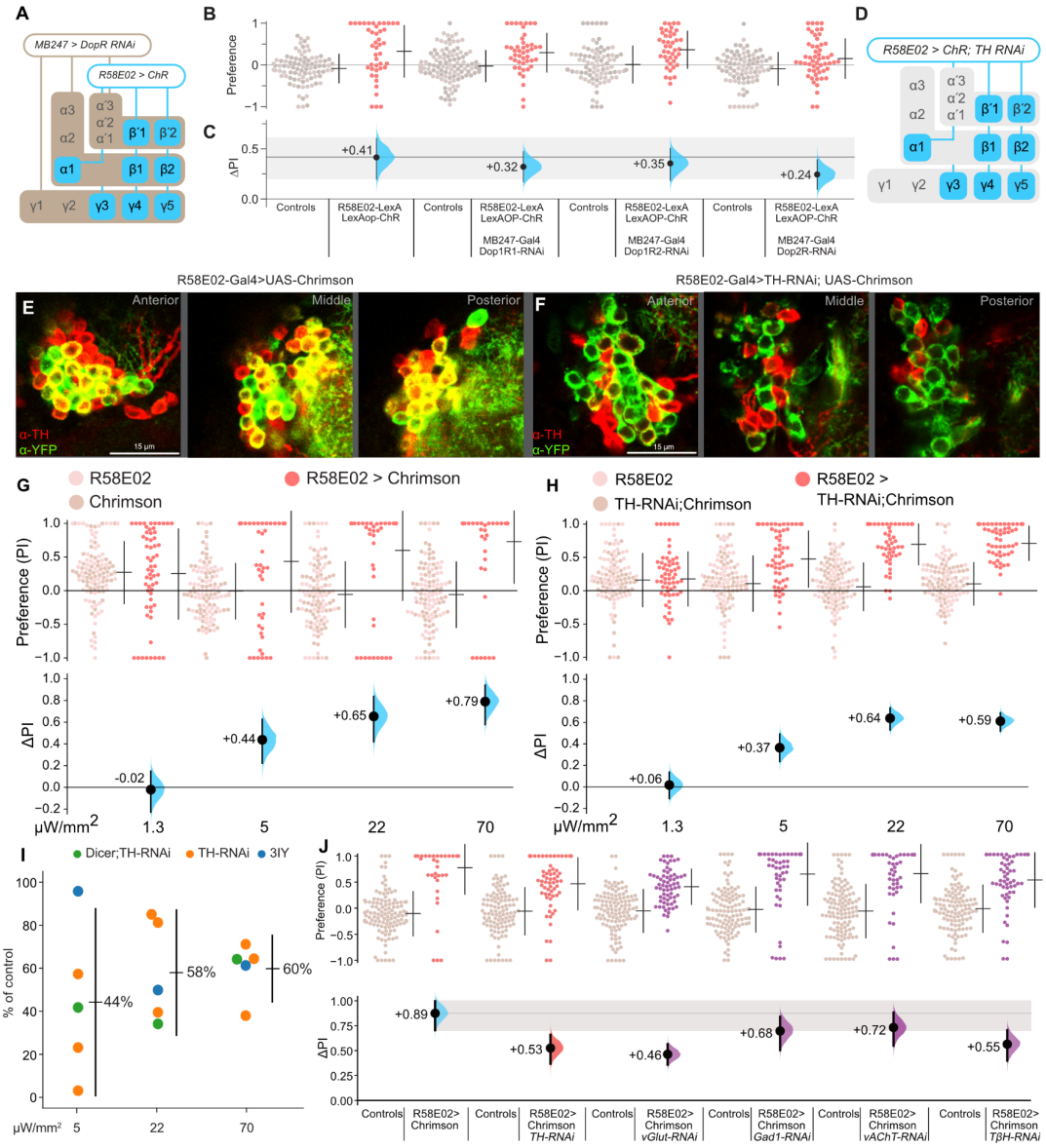

Figure 3. Dopamine is required for normal DAN-mediated attraction

A. Schematic illustrating the use of *MB247-Gal4* to use RNA interference to knock down receptor expression in the *R58E02-LexA>lexAop-Chr* optogenetic background.

B-C. Knocking down *Dop1R1*, *Dop1R2*, and *Dop2R* in the KCs had minor effects on *R58E02-LexA>lexAop-Chr* light attraction. The gray ribbon indicates the control-valence 95% confidence interval. Experiments used 72 µW/mm^2 red light.

D. Schematic for using *R58E02-Gal4* to simultaneously express Chrimson and knock down *TH* expression.

E. Immunohistochemistry of the PAM DAN cluster stained with α-TH (red) and α-YFP (green) in flies expressing Chr-YFP in the *R58E02* cells. Yellow rings indicate the co-localization of α-TH and α-YFP signals in cells in the PAM cell-body cluster at three optical slices.

F. Immunohistochemistry images of the DANs with TH-RNAi co-expression show that cells with α-YFP signal (*R58E02* cells) have a greatly lower α-TH signal.

G-H. Knocking down *TH* expression with TH-RNAi has a moderate effect on R58E02 valence across four intensities. For example, at 70 μW/mm^2 the valence is +0.79 ΔPI in *R58E02>Chr* flies (G) and is reduced to +0.59 ΔPI in flies carrying the *UAS-TH-RNAi* knockdown transgene (H).

I. Summary of the effects of reducing dopamine on *R58E02*-mediated valence with either gene knockdown (*UAS-TH-RNAi,* with or without *UAS-Dicer*) or a chemical inhibitor of TH activity (3-Iodo-L-tyrosine, 3IY). Each dot represents the percentage effect size of light intensity in an experiment (i.e., the *R58E02>Chr; TH-RNAi* experiment was replicated three times). Across all three intensities in five experiments, dopamine depletion resulted in an average ~46% reduction in valence. The vertical line indicates the 95% confidence interval.

J. A knockdown screen for neurotransmitters that contribute to *R58E02* valence. *R58E02>Chr* flies were crossed with RNAi transgenes targeting factors required for five transmitters: *TH* (dopamine, replicating the prior experiment), *vGlut* (glutamate), *GAD1* (GABA), *vAchT* (acetylcholine), and *TβH* (octopamine). The *vGlut* and *TβH* knockdowns showed a reduction in valence comparable to the *TH* knockdown.

Dopamine receptors in the KCs are dispensable to broad DAN attraction

For olfactory learning, dopamine receptor expression in the KCs is required [25,30,51]. To determine if this is also true for *R58E02* attraction, we knocked down the receptors *Dop1R1, Dop1R2,* and *Dop2R* in the KCs with RNAi transgenes [52]. For this, we used *R58E02-LexA* to drive *LexAop-Chr,* which, compared to *R58E02-Gal4*, yielded a relatively lower valence score. Individual knockdowns of all three receptors caused relatively minor reductions in valence (**Figure 3A-C**). This is consistent with the idea that *R58E02* valence is distinct from appetitive learning and that the KCs are not essential to *R58E02*-mediated valence.

Dopamine plays a partial role in *R58E02* valence

We aimed to estimate the extent to which *R58E02* valence has a requirement for dopamine. We depleted dopamine in the DANs with several methods. First, we used RNAi against tyrosine hydroxylase (TH), an essential enzyme for dopamine synthesis [53], encoded in flies by the *TH* gene (also referred to as *pale*). In *R58E02 > TH-RNAi* flies, immunohistochemical staining of the DANs showed that TH expression was markedly reduced (**Figure 3D-F, Movie S2-S3**). Compared to flies with intact TH expression (**Figure 3G**), flies with reduced TH in the *R58E02* DANs expressed substantially lower valence (**Figure 3H**). This partial valence reduction was observed in the three higher light intensities, and across three replications of this experiment (**Figure 3G-H, S3A-D**). We aimed to increase the RNAi transgene's efficacy with the simultaneous overexpression of Dicer2 endonuclease; this resulted in overall valence that was comparable to the RNAi alone (**Figure S3E, 3I**). Finally, we systemically depleted dopamine by feeding flies 3-iodotyrosine (3-IY), a competitive inhibitor of TH [54,55]. This pharmacological intervention also resulted in *R58E02>Chr* valence undergoing

a large partial reduction (**Figure S3F-G**). Averaging the results of all three interventions (*TH-RNAi* alone, *TH-RNAi* with *Dicer2*, and 3-IY) across three light intensities indicated that dopamine depletion reduces *R58E02*-mediated valence to 54% of control levels, i.e., an overall reduction of –46% (**Figure 3I**). So it appears that dopamine is mediating about half of *R58E02* valence.

Broad DAN attraction relies on glutamate and octopamine

We hypothesized that the dopamine-independent component of *R58E02* valence may depend on one or more other neurotransmitters. We knocked down genes involved in the synthesis or vesicular transport of four other transmitters: *vGlut* for glutamate, *Gad1* for GABA, *vAChT* for acetylcholine, and *Tβh* for octopamine. Of these, knockdown of *vGlut* and *Tβh* in the *R58E02* cells produced effects on valence that were comparable to the dopamine reduction (**Figure 3J**). This result supports the idea that *R58E02* valence also requires glutamate and octopamine.

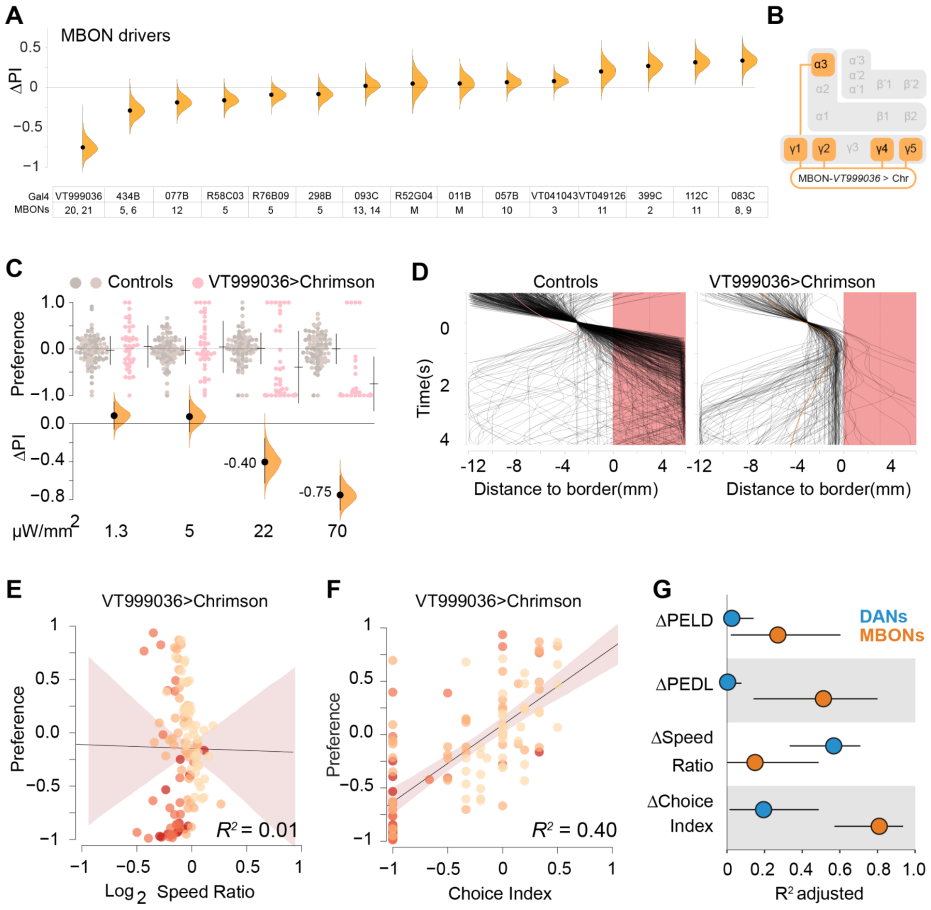

Figure 4. MBONs drive valence via choice effects, not speed effects.

A. A screen of optogenetic Chr valence in 15 MBON-related lines (split-Gal4 and Gal4 drivers). Orange markers show the valence scores (black dots) and distributions (curves) of each cross, comparing test flies with controls. See **Table S1** for effect sizes. The matrix key below shows driver identifiers in the top row, and MBON cell types in which each driver expresses; M denotes multiple cell types. See **Table S2** for further details.

B. A schematic of *VT999036* projections to MBON synaptic-zone subsets. The *VT999036* is reported to drive expression in two MBON types, MBON21 and MBON22 (also known as MBON-γ1γ2 and MBON-γ4γ5) [22].

C. *VT999036>Chr* flies avoided opto-activation at the two highest illumination intensities (22 and 70 μW/mm^2). The valence curve is the same data from the screen summary.

D. When *VT999036>Chr* flies move through the choicepoint, they tend to turn away from the light.

E. In *VT999036>Chr* flies, a relationship between preference and speed ratios was absent.

F. In *VT999036>Chr* flies, choice index and preference were related.

G. Summary of regressions of DAN and MBON driver valence. Coefficients of determination for DAN lines (blue dots) and MBON lines (orange dots) are shown for four locomotor metrics as compared to valence (ΔPreference). The four metrics are Δchoice, Δspeed ratio, and the effect sizes of the dark-light and light-dark choice-point exit probabilities (ΔPEDL and ΔPELD, respectively).

DANs and MBONs drive valence with different locomotion patterns

In the mushroom body, the MBONs are known to drive valence [27], and receive synaptic input from the DANs [56]. We asked whether the valence responses mediated by activating DANs and MBONs have similar locomotor features. Screening a panel of MBON drivers for valence (**Figure 4A, S4A-B**), one line, *VT999036*, was found to have the strongest valence. *VT999036* drives expression in MBONs that project to the γ lobe, termed MBON-γ1γ2 and MBON-γ4γ5 cells, also known as MBON types 21 and 22, respectively [22,35] (**Figure 4B, S4E-F, Table S2**). Activation of *VT999036* caused strong aversive valence that (in those flies that crossed from dark to light) was associated with turning away from the light at a light-dark boundary (**Figure 4C-D**). The dark preference of *VT999036>Chr* flies had little relationship to light–dark speed differences but was correlated with a choice index, i.e., fly trajectories at the boundary (**Figure 4E-F**). This contrasts with *R58E02>Chr* and *R15A04>Chr* flies, in which valence is correlated with speed (**Figure 1G-H, S1C-F**).

This observation led us to ask whether the speed/choice dissociation observed in the *R58E02* and *VT999036* lines was part of a trend for DAN and MBON lines generally. We analyzed metrics for all lines in the MBON and DAN screens (**Figure S4A-B, S5A-B**) and used them in regressions of the two screens' valence and speed ratio effect sizes. This analysis indicated that PAM-mediated valences were weakly determined by choice and strongly determined by speed differences (**Figure 4G, S4H-K, S5A-B**). In contrast, MBON-mediated valence was weakly associated with speed and more strongly determined by choice and choice-point exit probabilities (**Figure 4G, S4L-O**). Because lines for both neuronal categories can drive attraction and avoidance, this difference is not easily explained by valence polarity. Still, it suggests that MBON and DAN activities have differential effects on two navigational properties: turning and speed.

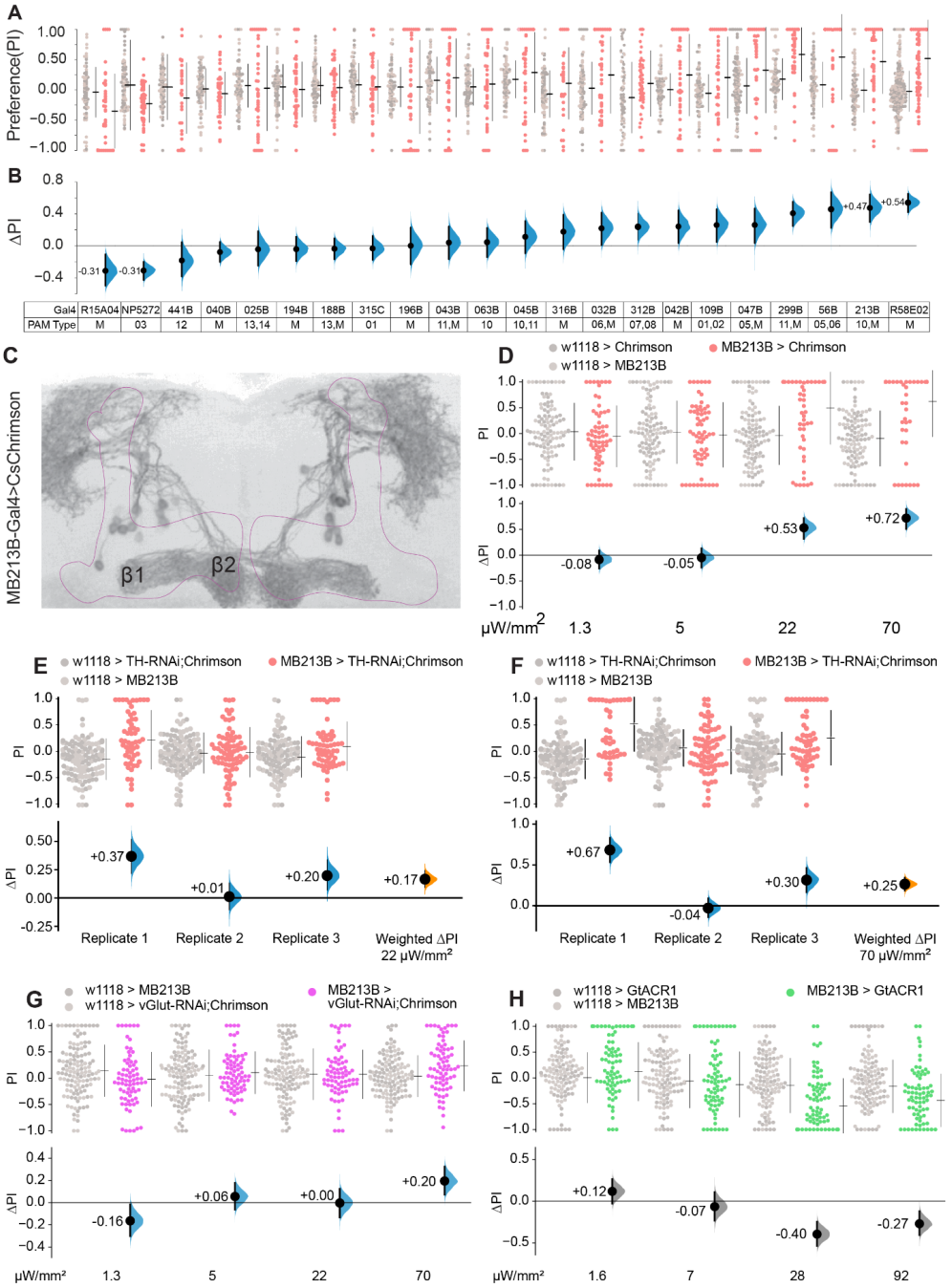

Figure 5. Valence mediated by dopaminergic β-lobe neurons is dependent on both dopamine and glutamate.

A-B. An optogenetic activation screen of 22 PAM-DAN lines identified *MB213B* as the specifically expressing line with the strongest positive valence. Light preference was tested with 72 μW/mm² red light. Table shows the PAM cell types in which each driver expresses; 'M' denotes multiple cell types. See **Table S2** for further details.

C. Expression pattern of *Chr-YFP* with driver *MB213B* showed projections to both zones of the β lobe (zones β1 and β2).

D. Replication of the *MB213B>Chr* screen experiment confirmed that these flies are attracted to optogenetic light at the two highest intensities.
E-F. Meta-analysis of three replicates of *MB213B > TH-RNAi; Chr* yielded weighted ΔPI values of +0.17 at 22 μW/mm^2 and +0.25 at 70 μW/mm^2 (orange curves).
G. Expressing vGlut-RNAi with the *MB213B* driver similarly resulted in reduced (but not ablated) valence.
H. *MB213>ACR1* flies avoided the green-illuminated area.

PAM-β valence is at least partially dependent on dopamine

The opposing valence of *R58E02* and *R15A04* suggested valence heterogeneity in different subsets of PAM DANs. Numerous studies have found that valence-related behaviors like food-seeking, courtship, sleep, and appetitive memory are dependent on different MB sub-compartments and specific DAN subsets [24,27,39,45,57–62]. To identify PAM types that drive valence, we screened twenty split-Gal4 lines [22,27] and identified several with valence, both negative and positive (**Figure 5A–B**). Of these lines, we focused on *MB213B* as it had the strongest positive valence (**Figure 5B**). This line expresses in the PAM-β1 and PAM-β2 types (PAM4 and PAM10, respectively) with minor expression in the PAM11 (PAM-α1) cells [22] (**Table S2**). Since valence in *R58E02>Chr* flies is only partially dependent on dopamine, we interrogated *MB213B>Chr* dopamine dependency. Knocking down *TH* in PAM-β cells produced variable results (**Figure S5C-E)**; to resolve these replicate differences, we used inverse-variance meta-analysis using a fixed-effects model to calculate weighted mean-difference estimates at the 22 and 70 μW/mm^2 light intensities [63]. These meta-analyses showed that, when compared to non-RNAi flies (**Figure 5D**), knockdown of *TH* produced a robust though incomplete valence reduction: –68% and –65%, respectively (**Figure 5E-F**). These effects are larger than the *TH-RNAi* knockdown effects for *R58E02>Chr*, which were –42% and –40% for the same light intensities (**Figure 3I**).

PAM-β valence is partially dependent on glutamate

The PAM-β cells have been shown via single-cell RNA-seq to express several other neurotransmitter-related genes, including *vGlut*, *vAChT,* and *Gad1* [39]. As glutamate appears to be a co-transmitter for *R58E02* valence, we examined the effect of *vGlut* knockdown in the specific driver. *MB213B > vGlut-RNAi; Chr* flies displayed valence that was reduced but, like the *TH* knockdown, not eliminated (**Figure 5G**). Thus, it appears that both glutamate and dopamine transmission contribute to valence mediated by the *MB213B* driver, likely through the PAM-β cells.

Pre-existing β-lobe DAN activity contributes to ongoing valence

We asked whether flies are responsive to inhibition of the *MB213B* cells [64]. To drive inhibition, we expressed ACR1 in the *MB213B* cells [49,50]. *MB213B>ACR1* flies displayed negative valence towards green light, indicating that the PAM-β cells are active during this simple behavioral task, and that this activity contributes to valent locomotion (**Figure 5H**).

Discussion

Differences between appetitive learning and acute DAN valence

In this study we provide evidence that a dopaminergic system known to instruct learning also drives acute valence. The PAM DANs instruct appetitive odor learning [12,51], such that subsequent encounters with the same odor will elicit increased approach behavior. Three features distinguish DAN-mediated olfactory learning from DAN-evoked acute valence. First, unlike classical Pavlovian learning—which requires an association between dopamine and a sensory stimulus—acute DAN valence occurs in an experimental environment that is otherwise largely featureless, such that the optogenetic illumination is the only salient sensory stimulus. Second, while the KCs are critical to DAN-mediated sensory associative learning [47,48], activated DAN acute valence has little to no reliance on KCs. Third, while learning has a complete dependency on dopamine receptors in the KCs [30,34,65], *R58E02* PAM valence does not have critical dependencies on either dopamine-receptor function in the KCs or PAM dopamine synthesis. Thus, DAN-dependent learning and DAN valence appear to be distinct processes that act through different circuits and signaling systems.

Differences between DAN and MBON valence

Previously, it was shown that PPL DANs are able to drive optogenetic valence behavior [56]. This study excluded the KCs as the downstream neurons through which the PAM DANs affect valence. This suggests the MBONs as possible mediators, since this class of neurons are major output cells of the MB [22,66–68], and receive synaptic input from the DANs [56].

Under the assumption that DAN valence is mediated by MBONs, we explored some features of valent locomotion as driven by the two cell types. The DAN lines primarily influenced optogenetic light preference by affecting walking speed, while the MBONs, as previously shown [27], had their primary effect by changing trajectories at the light–dark interface, a trend that was independent of valence polarity. There are at least four possible explanations for this difference. First, some of the driver lines (e.g. *VT999036*) capture cells without MB projections, and these could be contributing to valence, at least in some

cases. Second, DANs may have a symmetrical influence on walking, while the MBONs have an asymmetrical effect on walking, perhaps via an algorithm similar to those in Braitenberg vehicles [69]. Third, assuming that DAN valence is mediated by MBON activity, it may be that the MBONs have speed effects when quiescent, but drive turning when highly active, e.g., through distinct downstream circuits with distinct responsiveness to MBON activity. Fourth, the MBON screen may not have included the downstream cells responsible for DAN valence, i.e., other downstream circuits mediate the DAN effects. On this fourth point: the drivers that express in co-zonal DAN and MBON types do not necessarily specify cellular subtypes that share synapses [70,71].

The function of DAN→MBON interactions remains unknown, indeed it is not known whether the DANs drive valent locomotion through the MBONs. Moreover, the idea that DAN valences are exclusively mediated by DAN→MBON synapses in the MB is likely to be incorrect. Connectomic analysis has shown that the PAMs can have pre-synapses in other neuropils [71], suggesting that at least some of the valence effects could be mediated through PAM signaling to non-MB areas. In either case, the speed/turning dissociation is hard to explain with current information.

The appetitive DANs have non-conditioning functions

These results cast DAN-driven acute valence and olfactory sensory learning as separable processes, wherein the DANs bifurcate to perform two distinct functions. In response to rewarding (or punishing) stimuli, the PAM DANs appear to (1) write olfactory memories to Kandelian-type KC synapses for future reference, and (2) instruct immediate changes in locomotor behavior. Imaging of the MB has shown that DAN activity is closely connected with motor states and locomotion [24,72,73]. Inhibition experiments have revealed that DAN activities guide innate odor avoidance [74], and odor navigation [73]. Similarly, in mammals, reward-related behaviors can be separated into consummatory, motivational, and learning components, of which the latter two are attributable to dopamine function [75]. Organizing parallel signals of a single reward circuit into distinct motivational and associative dopaminergic synapses ensures coherence between valence (the present) and subsequent learned sensory responses (the future). From an evolutionary perspective, we speculate that the motor-function arm predates the associative arm [76], which was inserted when the first sensory systems (taste and olfaction) developed.

DAN valence relies on glutamate and octopamine

Knocking down *TH* function reduced *R58E02* valence by roughly half, suggesting the involvement of other neurotransmitters. Ablating four other

neurotransmitter pathways found that lesions in glutamate transport and octopamine synthesis also produced substantial reductions. Using the narrow driver *MB213B* which drives expression in the PAM-β cells, knockdowns revealed that dopamine and glutamate were required for normal valence. In previous studies, single-cell RNA sequencing revealed the co-expression of *vGlut*, *Gad1*, *vAChT* and *Tbh* in subpopulations of dopaminergic neurons [39,77]. Together, these findings indicate that the PAM DANs use dopamine, octopamine, and glutamate as co-transmitters.

Study limitations

Of this study's many limitations, of note is the sometimes pronounced variability in results between experimental iterations. For example, *R58E02 > Chr* flies showed variable valence when tested by different experimenters at different times (**Figure 1E, 3G**). Similarly, *MB213B > Chr; TH-RNAi* flies showed variable valence (**Figure S5C-E**). One likely contributor is routine sampling error [78]. For several dopamine-depletion experiments, we mitigated sampling error using meta-analysis to calculate a 'high-resolution' effect size ([78]. It is also possible that neurotransmitter dependencies may vary between iterations due to uncontrolled changes during development or internal state. For example, the loss of dopamine may sometimes lead to developmental compensation, such as neurotransmitter switching or circuit adjustments. In mammals, neurotransmitter switching in dopaminergic cells can occur as a result of stimuli such as odor or light stress [79–81]. In *Drosophila*, the expression of *vGlut* in DANs increases as dopamine is depleted either pharmacologically or due to aging [82]. It is possible that, as RNAi depletes TH, the PAM-β cells switch to glutamate as a substitute transmitter. Another possible explanation of the variability is that, due to one or more uncontrolled variables, some neurons' valence is susceptible to internal state. Imaging has shown that PAM-γ cells display activities that vary depending on state, such as starvation and walking [24,64]. If, for example, PAM-β baseline activity is high, it might be expected that the valence due to further activation will be small. Conversely, in a low baseline activity state, stimulation of these cells would be expected to result in a large effect.

Ongoing DAN activities shape behavior

That flies avoid silencing the PAM-β dopaminergic cells indicates that stimulus-independent DAN activities influence behavior. In the context of Pavlovian conditioning, dopamine has been closely associated with its role as a transient, stimulus-evoked signal, while this result indicates that some of the PAM neurons are active even in a chamber lacking food, odor, shock, or other stimuli. Physiological recordings show that, along with sucrose responses,

PAM-γ activities are correlated with motion and guide odor-tracking behavior, supporting the idea that PAM-DAN activities both respond to and steer locomotor behavior [24,73]. In our optogenetic preference screen, activity in various PAM DAN populations were rewarding, aversive or showed little preference effect, indicating that there is a diversity of functions between different DAN types, consistent with findings for learning and memory [12,14,18,31–39,51]. The bidirectionality of the attractive and aversive effects of increasing and decreasing activity in this dopaminergic system is similar to valence responses to activation and inhibition of dopaminergic cells in the mammalian ventral tegmental area [8,83,84] and is reminiscent of the increases and decreases in activity in that area that occur during positive and negative reward prediction errors, respectively [85]. Whole-brain imaging in the nematode has shown that global brain dynamics track closely with locomotion [86], suggesting that the primary overarching function of brains is to coordinate motor function. That the mushroom-body DANs drive preference-related locomotion suggest that they have two types of valence roles: informing responses to future experiences while steering current behavior.

Methods

Fly strains

Flies were cultured on a standard fly medium [87] at 25°C and 60% humidity in a 12 h light: 12 h dark cycle. Wild-type flies were a cantonized *w*^{1118} line. The DAN and MBON split-Gal4 lines described in [22] were a gift from Gerry Rubin (Howard Hughes Medical Institute), except for VT041043-Gal4 [88] and VT49126-Gal4 [35], which were obtained from the Vienna Drosophila Resource Center (VDRC). *VT999036* was a gift from Barry Dickson (Howard Hughes Medical Institute). The Gal4 transgenic lines were obtained from the Bloomington Drosophila Stock Center (BDSC) and included: *R58E02-Gal4* [13], *R15A04-Gal4* [43], *20x-UAS-CsChrimson* [40], 13X-LexAOp2-GtACR1 [89], *MB247-Gal4* [90], *MB247-LexA* [91]. *R53C03-Gal4* [22], *R76B09-Gal4* [35], *R52G04-Gal4* [27]. *NP5272-Gal4* [20] were obtained from the Kyoto Stock Center (DGRC). The RNAi lines used were: Dop1R1 (KK 107058), Dop1R2 (KK 105324), Dop2R (GD 11471), and TH (KK 108879), obtained from VDRC; as well as Gad1 (BDSC_51794), Tβh (BDSC_76062), and vAChT (BDSC_80435) from the Transgenic RNAi Project [92]. Supplemental Table 1 provides detailed descriptions of genotypes shown in each figure

Transgenic animal preparation

Gal4, *UAS-CsChrimson*, and *UAS-ACR1* crosses were maintained at 25°C and 60% humidity, in darkness. Groups of 25 newly eclosed flies were separated into vials for 2–3 days (in the dark at 25°C) before behavioral phenotyping. Control flies were generated by crossing the driver or responder line with a wild-type *w*^{1118} strain (originally bought from VDRC), and raising the progeny under identical regimes to those used for the test flies. A stock solution of all-*trans*-retinal was prepared in 95% ethanol (w/v) and mixed with warm, liquefied fly food. Each vial was covered with aluminum foil and incubated at 25°C in the dark. Before optogenetic experiments, 3–5 day-old male flies were fed 0.5 mM all-*trans*-retinal (Sigma) for 2–3 days at 25°C in the dark.

Drug treatment

Male flies (3–5 days old) were placed on 1% agar containing 5% sucrose, 10 mg/mL 3-iodo-L-tyrosine (3-IY, Sigma), and 0.5 mM all-trans-retinal for 2–3 days at 25°C in the dark prior to behavioral testing. Control flies were fed on the same food but with 3-IY omitted.

Immunohistochemistry

Immunohistochemistry was performed as previously described [50]. Briefly, brains were dissected in phosphate buffered saline (PBS) and fixed in PBS with 4% paraformaldehyde (Electron Microscopy Sciences) for 20 min. Samples were washed three times with PBT (PBS + 1% Triton X-100) and blocked with 5%

normal goat serum for 1 h. Samples were then incubated with primary antibodies overnight at 4°C. After three additional washes with PBT, samples were incubated with secondary antibodies overnight at 4°C. The following primary and secondary antibodies were used: mouse α-DLG1 (4F3 α-DISCS LARGE 1, Developmental Studies Hybridoma Bank, 1:200 dilution), Alexa Fluor 488 rabbit α-GFP-IgG (A-21311, Molecular Probes, 1:200 dilution), Alexa-Fluor 568 goat anti-mouse (1:200, Molecular Probes).

Confocal laser microscopy and neuroanatomy

Confocal images were acquired under a Zeiss LSM 710 microscope at a z-step of 0.5 µm using 20×, 40×, or 63× objectives. Images were analyzed using ImageJ software. Images are shown in black and white as a maximum projection intensity (MIP) of the green channel. The stacks were visualized and analyzed with the FIJI distribution (www.fiji.sc) of ImageJ (NIH). Outlines of α-Dlg1 expression in the mushroom body were traced with Adobe Illustrator. Projection patterns and zonal identity were assigned as previously described [22]. When not verified by microscopy, cell types and projection patterns were classified by review of published reports (Table S2) [22,35,36,45,51,88].

Optogenetic response assay

Behavior experiments were performed as previously described [50]. Each behavioral arena was cut with 55 × 4 mm stadium/discorectangle geometry; 15 such arenas were cut from 1.5 mm-thick transparent acrylic. During the behavioral assay, arenas were covered with a transparent acrylic lid. As previously described [3], flies were anesthetized on ice before loading into each chamber in the dark. The arena multiplex was kept under infrared (IR) light at 25°C for 2–3 min before starting the assay. Flies were aroused by shaking the arenas just before starting the experiment. All behaviors were recorded under IR light. The multiplex was illuminated with red or green light from a mini-projector positioned above the arena (Optoma ML750). For *CsChrimson* experiments, flies were illuminated with four red-light intensities: 1.3, 5, 22, and 70 µW/mm^2. For *ACR1* experiments, the flies were illuminated with four green light intensities: 1.6, 7, 28, and 92 µW/mm^2. The colored light intensity was varied by changing the level of the respective RGB component of the projected color. For each experiment, the arenas were illuminated for 60 s with equal-sized quadrants to produce a banded light-dark-light-dark pattern.

Video tracking

The behavior arena was imaged with a monochrome camera (Guppy-046 B, Allied Vision) with two IR longpass filters in series (IR Filter IR850, Green.L). Videos were processed in real time with CRITTA software written in LabView [50].

The x-y coordinates of each fly's head were individually tracked (at 25 frames per second) using CRITTA's tracking feature. CRITTA was also used to control the timing, hue and intensity of the illumination, and to count the number of flies in each quadrant for each video frame. The light borders were identified and calibrated using a function of the CRITTA plugin, which illuminates quadrants at low intensity and captures an image of the arenas (with camera IR filters removed). The plugin software calculates the horizontal intensity profile of each arena and finds the center of each light-dark boundary using an edge-detection algorithm. The light-border drift between presented experiments was 330 µm (95CI 230 µm; 430 µm). Between the light and dark regions, there is a light gradient that was a mean 670 µm wide with a range of 420 to 1040 µm. This was measured from 45 images of boundaries from 15 chambers, and scored as all the pixels falling between high (light-on) and low-intensity light regions.

Olfactory conditioning

Conditioning was performed as previously described [50,93]. Briefly, each behavior chamber was 50 mm long, 5 mm wide, and 1.3 mm high; the floor and ceiling of each chamber were composed of transparent shock boards made from indium tin oxide electrodes printed on glass (Visiontek UK). Odorized air was pumped into each end of each arena at 500 mL/min. The odors were 4-methylcyclohexanol (MCH) at 9 parts per million (ppm) and 3-octanol (OCT) at 6 ppm, as measured with a photoionization detector (RAE systems, ppbRAE3000). The air exited the chamber via two vents located in the middle, creating two odor partitions in the conditioning area. Each experiment was performed with 4–6 flies. For opto-conditioning, flies were presented with either OCT or MCH odor paired with green light (515 nm, 28 µW/mm^2), followed by another odor without visible light (IR light only). During shock-conditioning, the presentation of either OCT or MCH was coupled with 12 electric shocks of 1 s duration at 60V [18]. Conditioned-odor preference (memory) was tested by the presentation of both odors, one from each side. For each of the two odors, a half performance index (PI) was calculated according to the fly position coordinates during the last 30 s of each testing phase; for each iteration, data from odor pairs were averaged to obtain a full PI [94].

Preference and speed analysis

Custom Python scripts were used for data processing, analysis and visualization. The scripts integrated several routines from NumPy, pandas, matplotlib, and seaborn. For every fly, the x-y coordinates of the head location (recorded at 25 frames per second) underwent rolling-window smoothing, using a centered 1 s-wide triangular window. The following metrics were

obtained (for every fly) for the last 30 s of each test session:

$$Preference\ Index\ (PI) = \frac{time\ in\ light - time\ in\ dark}{total\ time}$$

$$log_2\ Speed\ Ratio\ (LSR) = log_2\left(\frac{mean\ speed\ in\ light}{mean\ speed\ in\ dark}\right)$$

While all flies could be assigned a PI, the log_2 Speed Ratio (LSR) could be computed only for flies that moved in both light and dark regions during the illumination epoch. Flies that remained stationary for the entire illumination epoch, or remained in only the light or dark zones, were excluded from the speed ratio calculation. Flies that start and remain in either the dark or light zone throughout an epoch, but still move within the zone, are assigned an extreme PI (–1.0 or +1.0, respectively).

Choice-zone trajectory analysis

A choice trajectory was defined as any transit in and out of a choice-zone defined to extend 3 mm in either direction from all three light borders. Trajectories were identified for every fly that approached the choice zone, and the following metrics were computed:

$$Choice\ Index\ (CI) = \frac{trajectories\ exiting\ to\ light - trajectories\ exiting\ to\ dark}{total\ trajectories}$$

$$Proportion\ of\ Exits\ from\ Dark\ to\ Light\ (PEDL) = \frac{entries\ from\ the\ dark\ exiting\ to\ light}{total\ entries\ from\ the\ dark}$$

$$Proportion\ of\ Exits\ from\ Light\ to\ Dark\ (PELD) = \frac{entries\ from\ the\ light\ exiting\ to\ dark}{total\ entries\ from\ the\ light}$$

The above three metrics were computed for all flies that entered a choice zone at least once during the illumination epoch. Flies that did not make such a crossing during the epoch (i.e. remained on one side for the epoch duration) were necessarily excluded from boundary trajectory analysis. Note that as flies can enter a choice zone without ever subsequently crossing from dark to light (or vice versa), not all flies with a choice index could also be assigned a speed ratio; this would include flies that consistently made choice-zone reversals without crossing a light-dark boundary. Thus, the choice-zone analysis necessarily excludes flies that never cross a light-dark boundary.

Effect-size regression

To compare the valence effect size (Δ Preference) with locomotion effect sizes, we calculated Δ values for four locomotion metrics.

$$\Delta\ Speed\ Ratio\ (\Delta LSR) = mean\ LSR_{test} - mean\ LSR_{control}$$

$$\Delta\ Choice\ Index\ (\Delta CI)\ =\ mean\ CI_{test} - mean\ CI_{control}$$

$$\Delta\ PELD\ =\ mean\ PELD_{test} -\ mean\ PELD_{control}$$

$$\Delta\ PEDL\ =\ mean\ PEDL_{test} -\ mean\ PEDL_{control}$$

Each Δ value was calculated for the two highest illumination intensity epochs (22 and 70 μW/mm2) for all PAM or MBON lines. As the locomotion metrics require that a fly crosses the light–dark boundary at least once, some flies were necessarily censored from this analysis.

Each set of effect sizes was subjected to regression against the corresponding Δ Preference values. Regression was performed with the linear least-squares method of the SciPy library. For both mean differences and coefficients of determination (R^2), distributions and 95% confidence intervals were obtained from 3,000 resamples, using bias correction and acceleration [95] with the scikits.bootstrap package.

Meta-analysis of dopamine-depleting interventions

Different dopamine loss-of-function experiments with *R58E02>Chr* were done using 3-iodo-tyrosine, *TH-RNAi*, or *TH-RNAi* with *Dicer2* at several light intensities, a total of 15 valence experiments. We aimed to estimate the effect of reducing dopamine function in the *R58E02* cells as a percentage of wild-type behavior [65,96]. Using data from three replicates of the *R58E02>Chr* experiment, we first calculated a mean ΔPI (controls) valence via simple averaging for the 5, 22 and 70 μW/mm^2 light conditions. The ΔPIs for each dopamine-depleting intervention were then expressed as a percentage of the control value [96] for each of three light intensities .

$$Mean\ \Delta PI\ of\ controls\ =\ \frac{\Sigma\ \Delta PI\ across\ 3\ replicates}{3}$$

$$Percent\ of\ control\ (\%\Delta PI)\ =\ \frac{Intervention\ \Delta PI}{Mean\ control\ \Delta PI} \times 100$$

The data used for calculating the mean ΔPI (controls) value is presented in **Figures 3G**, **S3D** and **S3E**. The data used for calculating % of control for each intervention is presented in figures: **S3B** (3-iodo-tyrosine); **3H**, **S3F** and **S3G** (*TH-RNAi*); **S3C** (*TH-RNAi* with *Dicer2*).

Meta-analysis of experimental replicates

For replicates of the *MB213> TH-RNAi; Chrimson* experiment, we performed inverse-variance meta-analysis with a fixed-effects model. A weighted effect size was calculated as follows:

$$\theta_{weighted} = \frac{\Sigma\,(\hat{\theta}_i w_i)}{\Sigma\, w_i}$$

Where:

$$\hat{\theta}_i = Effect\ size\ (mean\ difference)\ for\ replicate\ i$$

$$w_i = Weight\ for\ replicate\ i = \frac{1}{s_i^2}$$

$$s_i^2 = Pooled\ control + test\ variance\ for\ replicate\ i$$

Statistics

Effect sizes were used for data analysis and interpretation. Summary measures for each group were plotted as a vertical gapped line: the ends of the line correspond to the ±standard deviations of the group, and the mean itself plotted as a gap. Effect sizes were reported for each driver line as mean differences between controls and test animals for all the behavioral metrics [97]. Two controls (driver and responder) were grouped together and the averaged mean of the two controls was used to calculate the mean difference between control and test flies. In text form, the mean differences and their 95% confidence intervals are presented as "mean [95CI lower bound, upper bound]." The mean differences are depicted as black dots, with the 95% confidence interval indicated by error bars. Where possible, each error bar is accompanied with a filled curve displaying the distribution of mean differences, as calculated by bootstrap resampling. Bootstrapped distributions are robust for non-normal data [98].

P values were calculated by the Mann-Whitney rank method in SciPy and presented *pro forma* only: following best practice, no significance tests were conducted [97]. The behavioral sample sizes (typically *N* = 45, 45, 45) had a power of >0.8, assuming α = 0.05 and an effect size of Hedges' *g* = 0.6 SD. All error bars for mean differences represent the 95% confidence intervals.

Genotypes and statistics for control and test flies for each panel are provided in the Supplementary Table (**Table S1**), as are details of the mega-analysis of mutant effect sizes (**Figure 4G**) incorporating data from across the study.

Data and code availability

The data and code that support the findings of this study will be available from a Zenodo repository.

Acknowledgments

We thank Gerald Rubin (Howard Hughes Medical Institute) for the DAN and MBON split-Gal4 lines, Barry Dickson (Howard Hughes Medical Institute) for providing the *VT999036* flies. We thank Dr. Jessica Edwards of Insight Editing London for critical review of the manuscript before submission.

Author Contributions

Conceptualization: FM and ACC; Experiment design: FM, YM and ACC; Methodology: FM, JCS and ACC; Software: JH (Python), and JCS (CRITTA, LabView); Data Analysis: JH (Python), FM (Python), YM (Python) and JCS (LabView); Investigation: FM and YM (genetics, fly husbandry, behavior, immunohistochemistry, and microscopy), XYZ (behavior, brain dissection, immunohistochemistry, microscopy), SO (memory); Resources: JCS (instrumentation); Writing – Original Draft: FM; Writing – Revision: FM, YM, and ACC; Visualization: FM, YM, JH, ACC; Supervision: ACC; Project Administration: ACC; Funding Acquisition: ACC.

Competing interests

The authors declare no competing interests.

Funding

FM, YM, SO, XYZ, and ACC were supported by grants MOE-2013-T2-2-054, MOE2017-T2-1-089, and MOE2019-T2-1-133 from the Ministry of Education, Singapore; JCS and ACC were supported by grants 1231AFG030 and 1431AFG120 from the A*STAR Joint Council Office. YM was supported by Duke-NUS Medical School and by a President's Graduate Fellowship funded through the Jasmine Scholarship; JH was supported by the A*STAR Scientific Scholars Fund; SO was supported by a Khoo Postdoctoral Fellowship Award and an NMRC Young Investigator Research Grant; XYZ was supported by a Yong Loo Lin School of Medicine scholarship. The authors were supported by a Biomedical Research Council block grant to the Institute of Molecular and Cell Biology, and a Duke-NUS Medical School grant to ACC.

References

1. Anderson, D. J. & Adolphs, R. A framework for studying emotions across species. *Cell* **157**, 187–200 (2014).
2. Darwin, C. *The Expression of the Emotions in Man and Animals*. (Project Gutenberg, 1899).
3. Mohammad, F. *et al.* Ancient Anxiety Pathways Influence Drosophila Defense Behaviors. *Curr. Biol.* **26**, 981–986 (2016).
4. Bargmann, C. I. Beyond the connectome: how neuromodulators shape neural circuits. *Bioessays* **34**, 458–465 (2012).
5. Marder, E. Neuromodulation of neuronal circuits: back to the future. *Neuron* **76**, 1–11 (2012).
6. Schultz, W. Multiple dopamine functions at different time courses. *Annu. Rev. Neurosci.* **30**, 259–288 (2007).
7. Bromberg-Martin, E. S., Matsumoto, M. & Hikosaka, O. Dopamine in motivational control: rewarding, aversive, and alerting. *Neuron* **68**, 815–834 (2010).
8. Namburi, P., Al-Hasani, R., Calhoon, G. G., Bruchas, M. R. & Tye, K. M. Architectural Representation of Valence in the Limbic System. *Neuropsychopharmacology* **41**, 1697–1715 (2016).
9. Ueno, T. *et al.* Identification of a dopamine pathway that regulates sleep and arousal in Drosophila. *Nat. Neurosci.* **15**, 1516–1523 (2012).
10. Liu, Q., Liu, S., Kodama, L., Driscoll, M. R. & Wu, M. N. Two dopaminergic neurons signal to the dorsal fan-shaped body to promote wakefulness in Drosophila. *Curr. Biol.* **22**, 2114–2123 (2012).
11. Pimentel, D. *et al.* Operation of a homeostatic sleep switch. *Nature* **536**, 333–337 (2016).
12. Burke, C. J. *et al.* Layered reward signalling through octopamine and dopamine in Drosophila. *Nature* **492**, 433–437 (2012).
13. Liu, C. *et al.* A subset of dopamine neurons signals reward for odour memory in Drosophila. *Nature* **488**, 512–516 (2012).
14. Lin, S. *et al.* Neural correlates of water reward in thirsty Drosophila. *Nat. Neurosci.* **17**, 1536–1542 (2014).
15. Keleman, K. *et al.* Dopamine neurons modulate pheromone responses in Drosophila courtship learning. *Nature* **489**, 145–149 (2012).
16. Han, K. A., Millar, N. S., Grotewiel, M. S. & Davis, R. L. DAMB, a novel dopamine receptor expressed specifically in Drosophila mushroom bodies. *Neuron* **16**, 1127–1135 (1996).
17. Kim, Y.-C., Lee, H.-G. & Han, K.-A. D1 dopamine receptor dDA1 is required in the mushroom body neurons for aversive and appetitive learning in Drosophila. *J. Neurosci.* **27**, 7640–7647 (2007).
18. Claridge-Chang, A. *et al.* Writing memories with light-addressable reinforcement circuitry. *Cell* **139**, 405–415 (2009).

19. Schroll, C. *et al.* Light-Induced Activation of Distinct Modulatory Neurons Triggers Appetitive or Aversive Learning in Drosophila Larvae. *Curr. Biol.* **16**, 1741–1747 (2006).
20. Aso, Y. *et al.* Three dopamine pathways induce aversive odor memories with different stability. *PLoS Genet.* **8**, e1002768 (2012).
21. Busto, G. U., Cervantes-Sandoval, I. & Davis, R. L. Olfactory learning in Drosophila. *Physiology* **25**, 338–346 (2010).
22. Aso, Y. *et al.* The neuronal architecture of the mushroom body provides a logic for associative learning. *Elife* **3**, e04577 (2014).
23. Hige, T., Aso, Y., Modi, M. N., Rubin, G. M. & Turner, G. C. Heterosynaptic Plasticity Underlies Aversive Olfactory Learning in Drosophila. *Neuron* **88**, 985–998 (2015).
24. Cohn, R., Morantte, I. & Ruta, V. Coordinated and Compartmentalized Neuromodulation Shapes Sensory Processing in Drosophila. *Cell* **163**, 1742–1755 (2015).
25. Owald, D. & Waddell, S. Olfactory learning skews mushroom body output pathways to steer behavioral choice in Drosophila. *Curr. Opin. Neurobiol.* **35**, 178–184 (2015).
26. Lewis, L. P. C. *et al.* A Higher Brain Circuit for Immediate Integration of Conflicting Sensory Information in Drosophila. *Curr. Biol.* **25**, 2203–2214 (2015).
27. Aso, Y. *et al.* Mushroom body output neurons encode valence and guide memory-based action selection in Drosophila. *Elife* **3**, e04580 (2014).
28. Takemura, S.-Y. *et al.* A connectome of a learning and memory center in the adult Drosophila brain. *Elife* **6**, (2017).
29. Schwaerzel, M. *et al.* Dopamine and octopamine differentiate between aversive and appetitive olfactory memories in Drosophila. *J. Neurosci.* **23**, 10495–10502 (2003).
30. Kim, Y.-C., Lee, H.-G. & Han, K.-A. D1 dopamine receptor dDA1 is required in the mushroom body neurons for aversive and appetitive learning in Drosophila. *J. Neurosci.* **27**, 7640–7647 (2007).
31. Krashes, M. J. *et al.* A neural circuit mechanism integrating motivational state with memory expression in Drosophila. *Cell* **139**, 416–427 (2009).
32. Aso, Y. *et al.* Specific dopaminergic neurons for the formation of labile aversive memory. *Curr. Biol.* **20**, 1445–1451 (2010).
33. Aso, Y. *et al.* Three Dopamine Pathways Induce Aversive Odor Memories with Different Stability. (2012) doi:10.1371/journal.pgen.1002768.
34. Qin, H. *et al.* Gamma neurons mediate dopaminergic input during aversive olfactory memory formation in Drosophila. *Curr. Biol.* **22**, 608–614 (2012).
35. Shuai, Y. *et al.* Dissecting neural pathways for forgetting in Drosophila olfactory aversive memory. *Proc. Natl. Acad. Sci. U. S. A.* **112**, E6663–72 (2015).
36. Yamagata, N. *et al.* Distinct dopamine neurons mediate reward signals for short- and long-term memories. *Proc. Natl. Acad. Sci. U. S. A.* **112**, 578–583

(2015).

37. Aso, Y. & Rubin, G. M. Dopaminergic neurons write and update memories with cell-type-specific rules. *Elife* **5**, (2016).
38. Berry, J. A., Phan, A. & Davis, R. L. Dopamine Neurons Mediate Learning and Forgetting through Bidirectional Modulation of a Memory Trace. *Cell Rep.* **25**, 651–662.e5 (2018).
39. Aso, Y. *et al.* Nitric oxide acts as a cotransmitter in a subset of dopaminergic neurons to diversify memory dynamics. *Elife* **8**, (2019).
40. Klapoetke, N. C. *et al.* Independent optical excitation of distinct neural populations. *Nat. Methods* **11**, 338–346 (2014).
41. Nässel, D. R. & Elekes, K. Aminergic neurons in the brain of blowflies and Drosophila: dopamine- and tyrosine hydroxylase-immunoreactive neurons and their relationship with putative histaminergic neurons. *Cell Tissue Res.* **267**, 147–167 (1992).
42. Pfeiffer, B. D. *et al.* Tools for neuroanatomy and neurogenetics in Drosophila. *Proc. Natl. Acad. Sci. U. S. A.* **105**, 9715–9720 (2008).
43. Jenett, A. *et al.* A GAL4-driver line resource for Drosophila neurobiology. *Cell Rep.* **2**, 991–1001 (2012).
44. Perisse, E., Burke, C., Huetteroth, W. & Waddell, S. Shocking revelations and saccharin sweetness in the study of Drosophila olfactory memory. *Curr. Biol.* **23**, R752–63 (2013).
45. Huetteroth, W. *et al.* Sweet taste and nutrient value subdivide rewarding dopaminergic neurons in Drosophila. *Curr. Biol.* **25**, 751–758 (2015).
46. Ho, J., Tumkaya, T., Aryal, S., Choi, H. & Claridge-Chang, A. Moving beyond P values: data analysis with estimation graphics. *Nat. Methods* (2019) doi:10.1038/s41592-019-0470-3.
47. Dubnau, J., Grady, L., Kitamoto, T. & Tully, T. Disruption of neurotransmission in Drosophila mushroom body blocks retrieval but not acquisition of memory. *Nature* **411**, 476–480 (2001).
48. McGuire, S. E., Le, P. T. & Davis, R. L. The role of Drosophila mushroom body signaling in olfactory memory. *Science* **293**, 1330–1333 (2001).
49. Govorunova, E. G., Sineshchekov, O. A., Janz, R., Liu, X. & Spudich, J. L. Natural light-gated anion channels: A family of microbial rhodopsins for advanced optogenetics. *Science* **349**, 647–650 (2015).
50. Mohammad, F. *et al.* Optogenetic inhibition of behavior with anion channelrhodopsins. *Nat. Methods* (2017) doi:10.1038/nmeth.4148.
51. Liu, C. *et al.* A subset of dopamine neurons signals reward for odour memory in Drosophila. *Nature* **488**, 512–516 (2012).
52. Dietzl, G. *et al.* A genome-wide transgenic RNAi library for conditional gene inactivation in Drosophila. *Nature* **448**, 151–156 (2007).
53. Molinoff, P. B. & Axelrod, J. Biochemistry of catecholamines. *Annu. Rev. Biochem.* **40**, 465–500 (1971).

54. Bainton, R. J. *et al.* Dopamine modulates acute responses to cocaine, nicotine and ethanol in Drosophila. *Curr. Biol.* **10**, 187–194 (2000).
55. Neckameyer, W. S. Multiple roles for dopamine in Drosophila development. *Dev. Biol.* **176**, 209–219 (1996).
56. Takemura, S.-Y. *et al.* A connectome of a learning and memory center in the adult Drosophila brain. *Elife* **6**, (2017).
57. Sitaraman, D., Aso, Y., Rubin, G. M. & Nitabach, M. N. Control of Sleep by Dopaminergic Inputs to the Drosophila Mushroom Body. *Front. Neural Circuits* **9**, 73 (2015).
58. Montague, S. A. & Baker, B. S. Memory Elicited by Courtship Conditioning Requires Mushroom Body Neuronal Subsets Similar to Those Utilized in Appetitive Memory. *PLoS One* **11**, e0164516 (2016).
59. Tsao, C.-H., Chen, C.-C., Lin, C.-H., Yang, H.-Y. & Lin, S. Drosophila mushroom bodies integrate hunger and satiety signals to control innate food-seeking behavior. *Elife* **7**, (2018).
60. Dag, U. *et al.* Neuronal reactivation during post-learning sleep consolidates long-term memory in Drosophila. *Elife* **8**, (2019).
61. Handler, A. *et al.* Distinct Dopamine Receptor Pathways Underlie the Temporal Sensitivity of Associative Learning. *Cell* **178**, 60–75.e19 (2019).
62. Jacob, P. F. & Waddell, S. Spaced Training Forms Complementary Long-Term Memories of Opposite Valence in Drosophila. *Neuron* (2020) doi:10.1016/j.neuron.2020.03.013.
63. Borenstein, M., Hedges, L. V., Higgins, J. P. T. & Rothstein, H. R. *Introduction to Meta-Analysis*. (Wiley, 2009).
64. Siju, K. P. *et al.* Valence and State-Dependent Population Coding in Dopaminergic Neurons in the Fly Mushroom Body. *Curr. Biol.* **30**, 2104–2115.e4 (2020).
65. Tumkaya, T., Ott, S. & Claridge-Chang, A. Systematic review of Drosophila short-term-memory genetics: Meta-analysis reveals robust reproducibility. *Neurosci. Biobehav. Rev.* (2018) doi:10.1016/j.neubiorev.2018.07.016.
66. Tanaka, N. K., Tanimoto, H. & Ito, K. Neuronal assemblies of the Drosophila mushroom body. *J. Comp. Neurol.* **508**, 711–755 (2008).
67. Chiang, A.-S. *et al.* Three-dimensional reconstruction of brain-wide wiring networks in Drosophila at single-cell resolution. *Curr. Biol.* **21**, 1–11 (2011).
68. Owald, D. *et al.* Activity of defined mushroom body output neurons underlies learned olfactory behavior in Drosophila. *Neuron* **86**, 417–427 (2015).
69. Simões, J. M. *et al.* Robustness and plasticity in Drosophila heat avoidance. *Nat. Commun.* **12**, 2044 (2021).
70. Otto, N. *et al.* Input Connectivity Reveals Additional Heterogeneity of Dopaminergic Reinforcement in Drosophila. *Curr. Biol.* **30**, 3200–3211.e8 (2020).
71. Li, F. *et al.* The connectome of the adult Drosophila mushroom body

provides insights into function. *Elife* **9**, (2020).

72. Berry, J. A., Cervantes-Sandoval, I., Chakraborty, M. & Davis, R. L. Sleep Facilitates Memory by Blocking Dopamine Neuron-Mediated Forgetting. *Cell* **161**, 1656–1667 (2015).
73. Zolin, A. *et al.* Context-dependent representations of movement in Drosophila dopaminergic reinforcement pathways. *Nat. Neurosci.* **24**, 1555–1566 (2021).
74. Fuenzalida-Uribe, N. & Campusano, J. M. Unveiling the Dual Role of the Dopaminergic System on Locomotion and the Innate Value for an Aversive Olfactory Stimulus in Drosophila. *Neuroscience* **371**, 433–444 (2018).
75. Berridge, K. C. & Kringelbach, M. L. Pleasure systems in the brain. *Neuron* **86**, 646–664 (2015).
76. Llinas, R. R. *I of the Vortex: From Neurons to Self*. (MIT Press, 2001).
77. Croset, V., Treiber, C. D. & Waddell, S. Cellular diversity in the Drosophila midbrain revealed by single-cell transcriptomics. *Elife* **7**, (2018).
78. Cumming, G. & Calin-Jageman, R. *Introduction to the New Statistics: Estimation, Open Science, and Beyond*. (Routledge, 2016).
79. Dulcis, D. *et al.* Neurotransmitter Switching Regulated by miRNAs Controls Changes in Social Preference. *Neuron* **95**, 1319–1333.e5 (2017).
80. Dulcis, D., Jamshidi, P., Leutgeb, S. & Spitzer, N. C. Neurotransmitter switching in the adult brain regulates behavior. *Science* **340**, 449–453 (2013).
81. Meng, D., Li, H.-Q., Deisseroth, K., Leutgeb, S. & Spitzer, N. C. Neuronal activity regulates neurotransmitter switching in the adult brain following light-induced stress. *Proc. Natl. Acad. Sci. U. S. A.* **115**, 5064–5071 (2018).
82. Buck, S. A. *et al.* VGLUT modulates sex differences in dopamine neuron vulnerability to age-related neurodegeneration. *bioRxiv* 2020.11.11.379008 (2020) doi:10.1101/2020.11.11.379008.
83. Witten, I. B. *et al.* Recombinase-driver rat lines: tools, techniques, and optogenetic application to dopamine-mediated reinforcement. *Neuron* **72**, 721–733 (2011).
84. Danjo, T., Yoshimi, K., Funabiki, K., Yawata, S. & Nakanishi, S. Aversive behavior induced by optogenetic inactivation of ventral tegmental area dopamine neurons is mediated by dopamine D2 receptors in the nucleus accumbens. *Proc. Natl. Acad. Sci. U. S. A.* **111**, 6455–6460 (2014).
85. Schultz, W., Dayan, P. & Montague, P. R. A neural substrate of prediction and reward. *Science* **275**, 1593–1599 (1997).
86. Kato, S. *et al.* Global brain dynamics embed the motor command sequence of Caenorhabditis elegans. *Cell* **163**, 656–669 (2015).
87. Temasek Life Sciences Laboratories. Recipe for Drosophila media. *Zenodo* https://zenodo.org/record/1185451 (2018) doi:10.5281/zenodo.1185451.
88. Yang, C.-H. *et al.* Additive Expression of Consolidated Memory through Drosophila Mushroom Body Subsets. *PLoS Genet.* **12**, e1006061 (2016).

89. Jung, Y. *et al.* Neurons that Function within an Integrator to Promote a Persistent Behavioral State in Drosophila. *Neuron* **105**, 322–333.e5 (2020).
90. Zars, T., Fischer, M., Schulz, R. & Heisenberg, M. Localization of a short-term memory in Drosophila. *Science* **288**, 672–675 (2000).
91. Pitman, J. L. *et al.* A pair of inhibitory neurons are required to sustain labile memory in the Drosophila mushroom body. *Curr. Biol.* **21**, 855–861 (2011).
92. Perkins, L. A. *et al.* The Transgenic RNAi Project at Harvard Medical School: Resources and Validation. *Genetics* **201**, 843–852 (2015).
93. Kan, L. *et al.* A neural m6A/Ythdf pathway is required for learning and memory in Drosophila. *Nat. Commun.* **12**, 1458 (2021).
94. Tully, T. & Quinn, W. G. Classical conditioning and retention in normal and mutant Drosophila melanogaster. *J. Comp. Physiol. A* **157**, 263–277 (1985).
95. DiCiccio, T. J. & Efron, B. Bootstrap Confidence Intervals. *Stat. Sci.* **11**, 189–228 (1996).
96. Yildizoglu, T. *et al.* Estimating Information Processing in a Memory System: The Utility of Meta-analytic Methods for Genetics. *PLoS Genet.* **11**, e1005718 (2015).
97. Altman, D., Machin, D., Bryant, T. & Gardner, S. Statistics with confidence: confidence interval and statistical guidelines. *Bristol: BMJ Books* (2000).
98. Efron, B. & Tibshirani, R. J. *An Introduction to the Bootstrap*. (CRC Press, 1994).